

Improved analysis for $\mu^-e^- \rightarrow e^-e^-$ in muonic atoms by photonic interaction

Yuichi Uesaka¹, Yoshitaka Kuno¹, Joe Sato², Toru Sato^{1,3}, and Masato Yamanaka⁴

¹*Department of Physics, Osaka University, Toyonaka, Osaka 560-0043, Japan*

²*Physics Department, Saitama University, 255 Shimo-Okubo, Sakura-ku, Saitama, Saitama 338-8570, Japan*

³*J-PARC Branch, KEK Theory Center, Institute of Particle and Nuclear Studies, KEK, Tokai, Ibaraki 319-1106, Japan*

⁴*Maskawa Institute, Kyoto Sangyo University, Kyoto 603-8555, Japan*

(Dated: November 7, 2018)

Studies of the charged lepton flavor violating process of $\mu^-e^- \rightarrow e^-e^-$ in muonic atoms by the four Fermi interaction [Y. Uesaka *et al.*, Phys. Rev. D **93**, 076006 (2016)] are extended to include the photonic interaction. The wave functions of a muon and electrons are obtained by solving the Dirac equation with the Coulomb interaction of a finite nuclear charge distribution. We find suppression of the $\mu^-e^- \rightarrow e^-e^-$ rate over the initial estimation for the photonic interaction, in contrast to enhancement for the four Fermi interaction. It is due to the Coulomb interaction of scattering states and relativistic lepton wave functions. This finding suggests that the atomic number dependence of the $\mu^-e^- \rightarrow e^-e^-$ rate could be used to distinguish between the photonic and the four Fermi interactions.

I. INTRODUCTION

It has been well recognized that charged lepton flavor violation (CLFV) is important to search for new physics beyond the standard model. Rare processes of muons, such as $\mu^+ \rightarrow e^+\gamma$ [1], $\mu^+ \rightarrow e^+e^-e^+$ [2], and $\mu^- \rightarrow e^-$ conversion [3], have given the strongest constraints on new physics models of CLFV interactions [4, 5]. Furthermore, it is expected that experimental sensitivity can be significantly improved in near future measurements.

As a new promising process to search for CLFV interaction, $\mu^-e^- \rightarrow e^-e^-$ in a muonic atom was proposed [6]. For heavy atoms with large atomic numbers (Z), large enhancement of the $\mu^-e^- \rightarrow e^-e^-$ rate due to the Coulomb attraction of the lepton wave functions to a nucleus is expected. Another advantage for $\mu^-e^- \rightarrow e^-e^-$ is that it can probe both the four Fermi contact and the photonic interactions, as in the $\mu^+ \rightarrow e^+e^-e^+$ decay and $\mu^- \rightarrow e^-$ conversion. In $\mu^-e^- \rightarrow e^-e^-$, a sum of the energies of two electrons in the final state would be $m_\mu + m_e - B_\mu - B_e$, where m_μ and m_e are the masses of a muon and an electron, respectively, and B_μ and B_e are binding energies of the muon and electron in a muonic atom, respectively. The energy of each electron in the final state is about $m_\mu/2$, and they are emitted almost back-to-back. The search for $\mu^-e^- \rightarrow e^-e^-$ is proposed in the COMET Phase-I experiment at J-PARC, Japan [7]. This new process could be essential to identify the scenario of new physics via the addition of sterile neutrinos at near future experiments [8].

The initial work [6] showed that the atomic number (Z) dependence of the $\mu^-e^- \rightarrow e^-e^-$ transition rate is expected to be of Z^3 , owing to the probability density of the wave functions of the Coulomb-bound electrons at origin. This result was obtained by plane wave approximation of the outgoing electrons and non-relativistic approximation of the bound states. In our previous work [9] for the case of the four Fermi contact interaction, we have studied the Coulomb interaction for emitted electrons by solving the Dirac equation with a finite charge distribution of nuclei. It was found that the Coulomb interaction is important not only for the bound leptons but also for the electrons emitted. Moreover, relativistic Dirac wave functions of leptons with the Coulomb interaction of finite-ranged nuclear charge distribution were found to play an important role. As a result, the $\mu^-e^- \rightarrow e^-e^-$ rate increases on an atomic number Z stronger than Z^3 . For ^{208}Pb , the $\mu^-e^- \rightarrow e^-e^-$ rate can be enhanced about 7 times larger than the previous expectation [6]. Apparently, improved treatment of the Coulomb interaction should be made also for the photonic contribution of $\mu^-e^- \rightarrow e^-e^-$ process to obtain a complete picture of the $\mu^-e^- \rightarrow e^-e^-$ process.

In this work, we have made improved analyses for the $\mu^-e^- \rightarrow e^-e^-$ process for the photonic interaction. It is noticed that the photonic interaction consists of two vertices, the $\mu e \gamma^*$ CLFV interaction and the $e e \gamma^*$ electromagnetic interaction, together with long range photon propagators. Since an overlap integral of each vertex involves rapidly-oscillating scattering electrons and photon wave functions and long range Coulomb bound state wave functions, a careful numerical study for the photonic interaction is required. In Sec. II, we start from the effective CLFV interaction for the $\mu^-e^- \rightarrow e^-e^-$ process. The multipole expansion formula on the $\mu^-e^- \rightarrow e^-e^-$ rate is extended to the photonic interaction process. In Sec. III, the improved treatments of lepton wave functions for the photonic interaction, in particular the atomic number (Z) dependence of the rate, are discussed. Then, we propose a possibility to distinguish the photonic interaction from the four Fermi interaction, by the atomic number (Z) dependence and its angular-energy distribution of the emitted electrons. Our analysis is summarized in Sec. IV.

II. FORMULATION

A. Effective interaction

The effective Lagrangian for $\mu^- e^- \rightarrow e^- e^-$ consists of the photonic interaction $\mathcal{L}_{\text{photo}}$ and the four Fermi interaction $\mathcal{L}_{\text{contact}}$, as follows:

$$\mathcal{L}_{CLFV} = \mathcal{L}_{\text{photo}} + \mathcal{L}_{\text{contact}}, \quad (1)$$

where

$$\begin{aligned} \mathcal{L}_{\text{photo}} &= -\frac{4G_F}{\sqrt{2}} m_\mu [A_R \bar{e}_L \sigma^{\mu\nu} \mu_R + A_L \bar{e}_R \sigma^{\mu\nu} \mu_L] F_{\mu\nu} + [h.c.], \\ \mathcal{L}_{\text{contact}} &= -\frac{4G_F}{\sqrt{2}} [g_1 (\bar{e}_L \mu_R) (\bar{e}_L e_R) + g_2 (\bar{e}_R \mu_L) (\bar{e}_R e_L) \\ &\quad + g_3 (\bar{e}_R \gamma_\mu \mu_R) (\bar{e}_R \gamma^\mu e_R) + g_4 (\bar{e}_L \gamma_\mu \mu_L) (\bar{e}_L \gamma^\mu e_L) \\ &\quad + g_5 (\bar{e}_R \gamma_\mu \mu_R) (\bar{e}_L \gamma^\mu e_L) + g_6 (\bar{e}_L \gamma_\mu \mu_L) (\bar{e}_R \gamma^\mu e_R)] + [h.c.]. \end{aligned} \quad (2)$$

Here, $G_F = 1.166 \times 10^{-5} \text{GeV}^{-2}$ is the Fermi coupling constant, and $A_{L/R}$ and g_i ($i = 1, \dots, 6$) are the coupling constants which are determined by new physics models. The left- and right-handed fields $\psi_{L/R}$ are defined as $\psi_{L/R} = P_{L/R} \psi$, using the projection operators $P_{L/R} = (1 \mp \gamma_5)/2$.



FIG. 1. The diagrams representing $\mu^- e^- \rightarrow e^- e^-$: the one-photon-exchange photonic interaction (a) and the four Fermi contact interaction (b). The black closed circle shows the CLFV interaction.

The one-photon-exchange photonic interaction shown in Fig. 1 (a) is given by the photonic interaction in Eq. (2) together with the electromagnetic interaction of

$$\mathcal{L}_{em} = -q_e \bar{e} \gamma^\lambda e A_\lambda. \quad (4)$$

Here $q_e = -e$ is a charge of an electron. The four Fermi interaction shown in Eq. (3) and Fig. 1 (b) has been studied [9]. The transition amplitude M of $\mu^- e^- \rightarrow e^- e^-$ is given by,

$$2\pi i \delta(E_f - E_i) M(\mathbf{p}_1, s_1, \mathbf{p}_2, s_2; \alpha_\mu, s_\mu, \alpha_e, s_e) = \langle e_{\mathbf{p}_1}^{s_1} e_{\mathbf{p}_2}^{s_2} | T[\exp \left\{ i \int d^4 x (\mathcal{L}_{CLFV} + \mathcal{L}_{em}) \right\}] | \mu_{1S}^{s_\mu} e_{\alpha_e}^{s_e} \rangle, \quad (5)$$

with

$$M(\mathbf{p}_1, s_1, \mathbf{p}_2, s_2; \alpha_\mu, s_\mu, \alpha_e, s_e) = M_{\text{photo}}(\mathbf{p}_1, s_1, \mathbf{p}_2, s_2; \alpha_\mu, s_\mu, \alpha_e, s_e) + M_{\text{contact}}(\mathbf{p}_1, s_1, \mathbf{p}_2, s_2; \alpha_\mu, s_\mu, \alpha_e, s_e). \quad (6)$$

Here E_i and E_f are the energy of the initial and final state given as $E_i = m_\mu - B_\mu^{1S} + m_e - B_e^{\alpha_e}$ and $E_f = E_{p_1} + E_{p_2}$, respectively. And E_{p_i} is an energy of the electron with its momentum p_i and B_l^α is a binding energy of the lepton l in the state α . The principle quantum number n and κ [10, 11] of the bound muon and electron are collectively denoted by α_μ and α_e , respectively. We assume the initial muon is in its $1S_{1/2}$ ($n = 1$ and $\kappa = -1$) state, while we have included contribution of all bound electrons. The expression of M_{contact} is given as M in Eq. (4) of Ref. [9]. The amplitude of the photonic interaction M_{photo} is given as

$$\begin{aligned} M_{\text{photo}}(\mathbf{p}_1, s_1, \mathbf{p}_2, s_2; 1S, s_\mu, \alpha_e, s_e) &= \left[\frac{8G_F}{\sqrt{2}} m_\mu q_e \int d^3 x_1 d^3 x_2 G_\nu(\mathbf{x}_1, \mathbf{x}_2; m_\mu - B_\mu^{1S} - E_{p_1}) \right. \\ &\quad \times \bar{\psi}_{\mathbf{p}_1, s_1}^e(\mathbf{x}_1) \sigma^{\mu\nu} (A_L P_L + A_R P_R) \psi_{1S, s_\mu}^\mu(\mathbf{x}_1) \bar{\psi}_{\mathbf{p}_2, s_2}^e(\mathbf{x}_2) \gamma_\mu \psi_{\alpha_e, s_e}^e(\mathbf{x}_2) \left. \right] \\ &\quad - [\{\mathbf{p}_1, s_1\} \leftrightarrow \{\mathbf{p}_2, s_2\}]. \end{aligned} \quad (7)$$

The second term $\{\mathbf{p}_1, s_1\} \leftrightarrow \{\mathbf{p}_2, s_2\}$ is obtained by exchanging the quantum numbers of the final electrons in the first term. The photonic interaction is a finite range interaction between the two leptons and $G_\nu(\mathbf{x}_1, \mathbf{x}_2; q_0)$ is defined as

$$G_\nu(\mathbf{x}_1, \mathbf{x}_2; q_0) = \int \frac{d^3q}{(2\pi)^3} \frac{iq_\nu e^{-i\mathbf{q}\cdot(\mathbf{x}_1-\mathbf{x}_2)}}{|\mathbf{q}|^2 - q_0^2 - i\epsilon}. \quad (8)$$

B. Multipole expansion

To proceed, we derive a multipole expansion of the transition amplitude. Based on a standard partial wave expansion of the scattering wave functions and the bound state wave functions of Dirac particles given in Eqs. (11), (12), and (13) of Ref. [9], the transition amplitude is expressed as

$$\begin{aligned} M(\mathbf{p}_1, s_1, \mathbf{p}_2, s_2; 1S, s_\mu, \alpha_e, s_e) = & 2\sqrt{2}G_F \sum_{\kappa_1, \kappa_2, \nu_1, \nu_2, m_1, m_2} (4\pi)^2 (-i)^{l_{\kappa_1} + l_{\kappa_2}} e^{i(\delta_{\kappa_1} + \delta_{\kappa_2})} \\ & \times Y_{l_{\kappa_1}, m_1}(\hat{p}_1) Y_{l_{\kappa_2}, m_2}(\hat{p}_2) (l_{\kappa_1}, m_1, 1/2, s_1 | j_{\kappa_1}, \nu_1) (l_{\kappa_2}, m_2, 1/2, s_2 | j_{\kappa_2}, \nu_2) \\ & \times \sum_{J, M} (j_{\kappa_1}, \nu_1, j_{\kappa_2}, \nu_2 | J, M) (j_{-1}, s_\mu, j_{\kappa_e}, s_e | J, M) \\ & \times \frac{\sqrt{2(2j_{\kappa_1} + 1)(2j_{\kappa_2} + 1)(2j_{\kappa_e} + 1)}}{4\pi} N(J, \kappa_1, \kappa_2, E_{p_1}, \alpha_e), \end{aligned} \quad (9)$$

where $(l_\kappa, m, 1/2, s | j_\kappa, \nu)$ and $Y_{l_\kappa, m}(\hat{p})$ are the Clebsch-Gordan coefficients and the spherical harmonics, respectively. Here l_κ, j_κ are the orbital and the total angular momentum of the state with κ . δ_κ is a phase shift of the scattering state. The partial wave amplitude, $N(J, \kappa_1, \kappa_2, E_{p_1}, \alpha_e)$ for the photonic and the contact interactions is given by

$$N(J, \kappa_1, \kappa_2, E_{p_1}, \alpha_e) = N_{\text{photo}} + N_{\text{contact}}, \quad (10)$$

with

$$N_{\text{photo}} = \sum_{i=L/R} A_i W_i(J, \kappa_1, \kappa_2, E_{p_1}, \alpha_e) \quad (11)$$

$$N_{\text{contact}} = \sum_{i=1}^6 g_i W_i(J, \kappa_1, \kappa_2, E_{p_1}, \alpha_e). \quad (12)$$

Here W_i s ($i = 1, 2, \dots, 6$) for the contact interaction are given in Ref. [9]. The amplitudes of the photonic interaction $W_{L/R}$ are given as

$$W_{L/R} = \frac{2m_\mu}{i} \sqrt{\pi\alpha} \sum_{l=0}^{\infty} \sum_{j=|l-1|}^{l+1} \sum_{\lambda=1}^3 [X_\lambda(l, j, \kappa_1, \kappa_2, J) \pm iY_\lambda(l, j, \kappa_1, \kappa_2, J)], \quad (13)$$

where \pm corresponds to L and R , respectively. X_λ and Y_λ are expressed in terms of Z as

$$X_1(l, j, \kappa_1, \kappa_2, J) = (-1)^{l+j} \left\{ Z_{gfgf}^{l, l, 1, j}(J) + Z_{fggf}^{l, l, 1, j}(J) - Z_{gffg}^{l, l, 1, j}(J) - Z_{ffgf}^{l, l, 1, j}(J) \right\}, \quad (14)$$

$$X_2(l, j, \kappa_1, \kappa_2, J) = f_{l-j}^{(2)}(j) \left\{ Z_{gfgg}^{l, j, 0, j}(J) + Z_{fggg}^{l, j, 0, j}(J) + Z_{gfff}^{l, j, 0, j}(J) + Z_{ffgf}^{l, j, 0, j}(J) \right\}, \quad (15)$$

$$X_3(l, j, \kappa_1, \kappa_2, J) = f_{l-j}^{(3)}(j) \sum_{\{l_a, l_b\}=\{l, j\}, \{j, l\}} \left\{ Z_{gggf}^{l_a, l_b, 1, j}(J) - Z_{ffgf}^{l_a, l_b, 1, j}(J) - Z_{gfgf}^{l_a, l_b, 1, j}(J) + Z_{fffg}^{l_a, l_b, 1, j}(J) \right\}, \quad (16)$$

$$Y_1(l, j, \kappa_1, \kappa_2, J) = (-1)^{l+j} \left\{ Z_{gggf}^{l, l, 1, j}(J) - Z_{ffgf}^{l, l, 1, j}(J) - Z_{gfgf}^{l, l, 1, j}(J) + Z_{fffg}^{l, l, 1, j}(J) \right\}, \quad (17)$$

$$Y_2(l, j, \kappa_1, \kappa_2, J) = f_{l-j}^{(2)}(j) \left\{ Z_{gggg}^{l, j, 0, j}(J) - Z_{ffgg}^{l, j, 0, j}(J) + Z_{gfff}^{l, j, 0, j}(J) - Z_{ffff}^{l, j, 0, j}(J) \right\}, \quad (18)$$

$$Y_3(l, j, \kappa_1, \kappa_2, J) = f_{l-j}^{(3)}(j) \sum_{\{l_a, l_b\}=\{l, j\}, \{j, l\}} \left\{ Z_{gfgf}^{l_a, l_b, 1, j}(J) + Z_{fgfg}^{l_a, l_b, 1, j}(J) - Z_{gfgf}^{l_a, l_b, 1, j}(J) - Z_{ffgf}^{l_a, l_b, 1, j}(J) \right\}, \quad (19)$$

where

$$f_h^{(2)}(j) = \begin{cases} \sqrt{\frac{j+1}{2j+1}} & (h = +1) \\ 0 & (h = 0) \\ \sqrt{\frac{j}{2j+1}} & (h = -1) \end{cases}, \quad f_h^{(3)}(j) = \begin{cases} \sqrt{\frac{j}{2j+1}} & (h = +1) \\ 0 & (h = 0) \\ -\sqrt{\frac{j+1}{2j+1}} & (h = -1) \end{cases}. \quad (20)$$

The matrix element Z , which consists of CLFV and the electromagnetic vertex and the photon propagator is given by,

$$\begin{aligned} Z_{ABCD}^{l_a, l_b, s, j}(J) \equiv & \left[q_0^2 \int_0^\infty dr_1 r_1^2 A_{p_1}^{\kappa_1}(r_1) B_{1, \mu}^{\kappa_\mu}(r_1) \int_0^\infty dr_2 r_2^2 F_{l_a, l_b}^{q_0}(r_1, r_2) C_{p_2}^{\kappa_2}(r_2) D_{n, e}^{\kappa_e}(r_2) \right. \\ & \times (-1)^{J+\kappa_2+\kappa_e} V_{l_a, 1, j}^{s_A \kappa_1, s_B \kappa_\mu} V_{l_b, s, j}^{s_C \kappa_2, s_D \kappa_e} W(j_{\kappa_1} j_{\kappa_2} 1/2 j_{\kappa_e}; Jj) \\ & \left. - (-1)^{j_{\kappa_1} + j_{\kappa_2} - J} [\{p_1, \kappa_1\} \leftrightarrow \{p_2, \kappa_2\}] \right], \end{aligned} \quad (21)$$

where $\kappa_\mu = -1$ and $W(abcd; ef)$ is the Racah coefficient. Here, $A_p^\kappa(r)$, $C_p^\kappa(r)$ and $B_{n, \mu}^\kappa(r)$, $D_{n, e}^\kappa(r)$ are radial wave functions of the scattering states (g_p^κ, f_p^κ) and the bound states ($g_{n, l}^\kappa, f_{n, l}^\kappa$) given in Appendix and $s_A = \pm 1$ for $A = g$ and $A = f$, respectively. q_0 is $q_0 = m_\mu - B_\mu^{1S} - E_{p_1}$ for the direct term, and $q_0 = m_\mu - B_\mu^{1S} - E_{p_2}$ for the exchange term. The partial wave expansion of the photon propagator is given as

$$\int \frac{d^3 q}{(2\pi)^3} \frac{q_\nu e^{-i\mathbf{q} \cdot (\mathbf{x}_1 - \mathbf{x}_2)}}{|\mathbf{q}|^2 - q_0^2 - i\epsilon} = q_0 \partial_\nu \sum_{l, m} Y_{l, m}^*(\hat{x}_1) Y_{l, m}(\hat{x}_2) F_{l, l}^{q_0}(x_1, x_2), \quad (22)$$

where we have defined $\partial_\nu = (iq_0, \nabla_1)$ and

$$F_{l_1, l_2}^{q_0}(x_1, x_2) = h_{l_1}^{(1)}(q_0 x_1) j_{l_2}(q_0 x_2) \theta(x_1 - x_2) + h_{l_2}^{(1)}(q_0 x_2) j_{l_1}(q_0 x_1) \theta(x_2 - x_1). \quad (23)$$

Here j_l and $h_l^{(1)}$ are the spherical Bessel function and the first kind spherical Hankel function, respectively. The radial integral of the CLFV vertex is extended in a range of the Bohr radius of the muon, while the integrand extends to the electron Bohr radius for the electromagnetic vertex. Since the wave length of the electron scattering state around 50MeV is about 1/4 fm, a numerical integration for this radial integral is carefully made. The coefficient V s are given by reduced matrix elements of the spin-orbital wave function by;

$$\begin{aligned} V_{l, s, j}^{\kappa_b, \kappa_a} = & (-1)^l \frac{1 + (-1)^{l_{\kappa_b} + l_{\kappa_a} + l}}{2} (j_{\kappa_b}, 1/2, j_{\kappa_a}, -1/2 | j, 0) \\ & \times \begin{cases} \delta_{l, j} & (s = 0, j = l) \\ (j - \kappa_a - \kappa_b) / \sqrt{j(2j+1)} & (s = 1, j = l+1) \\ (\kappa_a - \kappa_b) / \sqrt{j(j+1)} & (s = 1, j = l) \\ -(j+1 + \kappa_a + \kappa_b) / \sqrt{(j+1)(2j+1)} & (s = 1, j = l-1) \end{cases}. \end{aligned} \quad (24)$$

Finally, the angular and energy distributions of the emitted electron are expressed in terms of the partial wave amplitude by

$$\begin{aligned} \frac{d^2 \Gamma_{\alpha_e}}{dE_{p_1} d \cos \theta} = & \frac{G_F^2}{2\pi^3} |\mathbf{p}_1| |\mathbf{p}_2| \sum_{\kappa_1, \kappa_2, \kappa'_1, \kappa'_2, J, l} (2J+1)(2j_{\kappa_e}+1)(2j_{\kappa_1}+1)(2j_{\kappa_2}+1)(2j_{\kappa'_1}+1)(2j_{\kappa'_2}+1) \\ & \times \frac{1 + (-1)^{l_{\kappa_1} + l_{\kappa'_1} + l}}{2} \frac{1 + (-1)^{l_{\kappa_2} + l_{\kappa'_2} + l}}{2} i^{-l_{\kappa_1} - l_{\kappa_2} + l_{\kappa'_1} + l_{\kappa'_2}} e^{i(\delta_{\kappa_1} + \delta_{\kappa_2} - \delta_{\kappa'_1} - \delta_{\kappa'_2})} \\ & \times (j_{\kappa_1}, 1/2, j_{\kappa'_1}, -1/2 | l, 0) (j_{\kappa_2}, 1/2, j_{\kappa'_2}, -1/2 | l, 0) W(j_{\kappa_1} j_{\kappa_2} j_{\kappa'_1} j_{\kappa'_2}; Jl) \\ & \times (-1)^{J - j_{\kappa_2} - j_{\kappa'_2}} N(J, \kappa_1, \kappa_2, E_{p_1}, \alpha_e) N^*(J, \kappa'_1, \kappa'_2, E_{p_1}, \alpha_e) P_l(\cos \theta), \end{aligned} \quad (25)$$

where $P_l(x)$ is Legendre polynomials. The total rate can be calculated by integrating the energy and angle:

$$\Gamma = \frac{1}{2} \sum_{\alpha_e} \int_{m_e}^{m_\mu - B_\mu^{1S} - B_e^{\alpha_e}} dE_{p_1} \int_{-1}^1 d \cos \theta \frac{d^2 \Gamma_{\alpha_e}}{dE_{p_1} d \cos \theta}. \quad (26)$$

After taking into account the approximations employed in Ref. [6], the above formula for the photonic interaction can be reduced to the following transparent formula of,

$$\Gamma_0(\mu^- e^- \rightarrow e^- e^-) = \frac{8m_e}{\pi}(Z-1)^3\alpha^4(G_F m_\mu^2)^2(|A_R|^2 + |A_L|^2). \quad (27)$$

III. RESULTS

The wave functions of the bound muon and electron and the emitted electrons in the final state are obtained by solving Dirac equations with the Coulomb potential numerically. We use the uniform nuclear charge distribution, $\rho_C(r)$, for the Coulomb potential, which is given as

$$\rho_C(r) = \frac{3Ze}{4\pi R^3}\theta(R-r), \quad (28)$$

with $R = 1.2A^{1/3}\text{fm}$. We have also examined a realistic charge distribution of the Woods-Saxon form. However the rate changes by less than 1% from that of the uniform distribution. Therefore the uniform charge distribution is decided to use in our calculation from now on. A sufficiently large number of partial waves of the scattering electron state has to be included. The convergence property of the rate against partial waves is shown in Table I. The

TABLE I. The convergence property of Γ/Γ_0 . The maximum values of $|\kappa|$ included for the rates in each column are given in the first row.

Nuclei	$ \kappa \leq 1$	$ \kappa \leq 5$	$ \kappa \leq 10$	$ \kappa \leq 20$
⁴⁰ Ca	0.0762	0.482	0.641	0.663
¹²⁰ Sn	0.125	0.396	0.406	0.406
²⁰⁸ Pb	0.109	0.270	0.271	0.271

convergence property is almost the same as the contact interaction. For ⁴⁰Ca, we have to sum the partial waves up to $|\kappa| \leq 20$. For larger Z nuclei, the rate converges faster due to a smaller radius of the bound muon.

For the photonic interaction, the effective interaction is not local due to the propagation of virtual photons. In principle, the bound electrons other than 1S state could contribute to the rate. The contributions to the rate from each atomic orbit, normalized to those of 1S state, are shown in Table II. It is found the contributions of the non-S wave bound electrons are larger than that of the contact interaction. However it is still very small, compared with those of 1S electrons. The total rate for ²⁰⁸Pb is enhanced by about 20% by including the electrons other than the 1S state.

TABLE II. The relative contributions to the rate from electrons in different atomic orbits under the M shell and the $4S$ orbit, for ²⁰⁸Pb. The spins are summed over. They are normalized by the 1S contribution.

1S	2S	2P	3S	3P	3D	4S	Total
1	0.15	7.3×10^{-3}	4.3×10^{-2}	2.6×10^{-3}	2.5×10^{-5}	1.8×10^{-2}	1.21

A. Rate of the photonic interaction

The ratio of the $\mu^- e^- \rightarrow e^- e^-$ rates, Γ/Γ_0 , is studied to examine the roles of Coulomb interaction of the scattering state and the relativistic wave function of the bound states. For simplicity, we set $A_R = 0$ and start discussions including only the contribution of the 1S electron bound state. We introduce three models summarized in Table III. In the model I, the scattering electrons are plane waves (PLW) and the wave function of bound electron is non-relativistic (Non. Rel.). The ratio of Γ/Γ_0 is shown in a dashed line of Fig. 2. Due to the finite size of the muon wave function, it is decreasing linearly as Z , even though the approximation for the lepton wave functions are the same in this work and Ref. [6]. This is observed in our previous work [9] for the contact interaction. In the model II, we replaced the bound state wave functions in the model I by relativistic one (Rel.). The result is shown in a

dash-two-dotted line. The relativistic effect of a bound electron at small distance makes the overlap integral larger and the ratio becomes $1 \sim 1.2$. Finally, we use the Coulomb distorted wave (DW) for the electron scattering state in the model III. The ratio is shown in a solid line. By taking into account the Coulomb distortion and the relativistic bound state wave functions, the rate is strongly suppressed compared with Γ_0 , which is quite different from large enhancement obtained for the contact interaction. The ratio is 0.27 (0.66) for ^{208}Pb (^{40}Ca).

TABLE III. Models for the electron wave functions. The relativistic bound state wave function (Rel.) and distorted wave of the scattering state (DW) are calculated in by the Coulomb potential from an uniform nuclear charge density. The non-relativistic bound state wave function (Non.) is obtained by using a point charge density.

Model	Bound electron	Scattering electron
I	Non. Rel.	PLW
II	Rel.	PLW
III	Rel.	DW

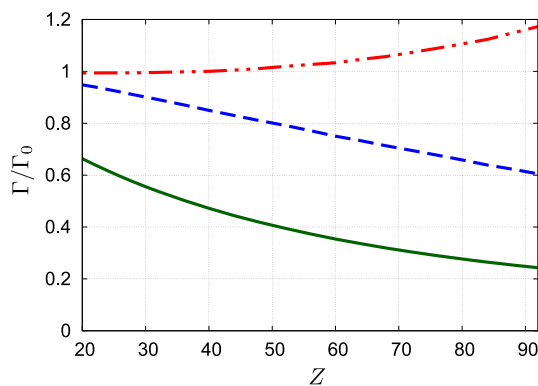


FIG. 2. The Z dependence of Γ/Γ_0 . The ratios Γ/Γ_0 of model I, II and III are shown in dashed, dash-two-dotted, and solid curves.

To understand the mechanism of the suppression of the $\mu^-e^- \rightarrow e^-e^-$ rate, we study a typical transition density,

$$\rho_{\text{tr}}(r) = j_0(q_0 r) g_{p_1}^{-1}(r) g_{1,\mu}^{-1}(r), \quad (29)$$

which indicates the partial transition density of a bound muon (1S) to a scattering electron ($\kappa = -1$) and a photon ($l = 0$). Here we select the most important kinematical region $p_1 = (m_\mu - B_\mu)/2 = q_0$, ignoring the electron mass. The transition densities calculated by using the PLW and DW electron wave functions are shown in Fig. 3. In the PLW case, ρ_{tr} is positive definite, since the wave length of the scattering electrons is the same as that of virtual photons. On the other hand, ρ_{tr} changes its sign and oscillates because of the Coulomb attraction for the electron. The same mechanism also can be applied to the vertex of the bound electron transition. Therefore the distortion of final electrons suppresses the transition rate.

In terms of the momentum space, the suppression of the $\mu^-e^- \rightarrow e^-e^-$ rate for the photonic interaction can be understood as follows. The momenta of the electron and virtual photon are transferred to the bound muon or the electron at each vertex for the photonic interaction. Main contribution to the rate is when the both electron and virtual photons carry about a half of the muon mass, so that the momentum transfer to the bound states is almost zero. While this is true for the asymptotic momentum of the electron, the Coulomb attraction increases local momentum of the electrons being close to the nucleus. This brings a mismatch of the virtual photon and the electron momenta and increases the momentum transfer to the bound leptons and hence the transition probability is reduced. A similar suppression mechanism of the transition rate was pointed out in Ref. [12] for the $\mu^- \rightarrow e^-$ conversion process.

The branching ratio of $\mu^-e^- \rightarrow e^-e^-$ by the photonic interaction is given as

$$Br(\mu^-e^- \rightarrow e^-e^-) \equiv \tilde{\tau}_\mu \Gamma(\mu^-e^- \rightarrow e^-e^-), \quad (30)$$

where $\tilde{\tau}_\mu$ is a mean life time of the muonic atom, given in Ref. [13]. The upper limit of this branching ratio is calculated by using A_R and A_L , which are constrained from the experimental upper limit of $\mu^+ \rightarrow e^+\gamma$. The branching ratio

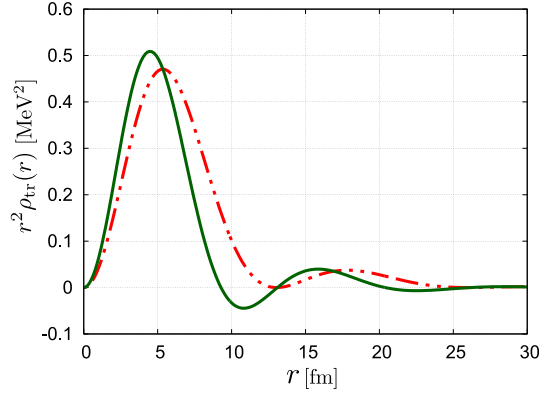


FIG. 3. The transition density $r^2\rho_{\text{tr}}(r)$ for ^{208}Pb . The dash-two-dotted and solid curves show the transition density using PLW and DW scattering electron, respectively. Here, the bound muon is treated relativistically in both curves.

$Br(\mu^+ \rightarrow e^+\gamma) = \Gamma(\mu^+ \rightarrow e^+\gamma)/\Gamma(\mu^+ \rightarrow e^+\bar{\nu}_\mu\nu_e)$ is given as

$$Br(\mu^+ \rightarrow e^+\gamma) = 384\pi^2 (|A_R|^2 + |A_L|^2). \quad (31)$$

Assuming the dominance of the photonic interaction, the upper limit of $Br(\mu^-e^- \rightarrow e^-e^-)$ can be expressed by using B_{max} , which is current upper limit of $Br(\mu^+ \rightarrow e^+\gamma)$ as,

$$\begin{aligned} Br(\mu^-e^- \rightarrow e^-e^-) &< \frac{Br(\mu^-e^- \rightarrow e^-e^-)}{Br(\mu^+ \rightarrow e^+\gamma)} B_{\text{max}} \\ &= 4(Z-1)^3 \alpha^4 \frac{m_e \tilde{\tau}_\mu}{m_\mu \tau_\mu} \frac{\Gamma(\mu^-e^- \rightarrow e^-e^-)}{\Gamma_0(\mu^-e^- \rightarrow e^-e^-)} B_{\text{max}}, \end{aligned} \quad (32)$$

where τ_μ is the mean life time of a free muon. The upper limit of the branching ratio (Eq. (32)) is calculated as a function of Z by using $B_{\text{max}} = 4.2 \times 10^{-13}$ by the MEG experiment [1]. The dashed (blue) line in Fig. 4 shows the result of previous work [6], whereas the results of this work with taking into account the 1S electrons and all the bound electrons are shown in a solid (red) and dotted (orange) lines, respectively. From the improved estimations using the relativistic Coulomb lepton wave functions, the branching ratio $Br(\mu^-e^- \rightarrow e^-e^-)$ is about 10^{-19} for ^{208}Pb . The non-1S bound electrons increase the branching ratio by about 20%.

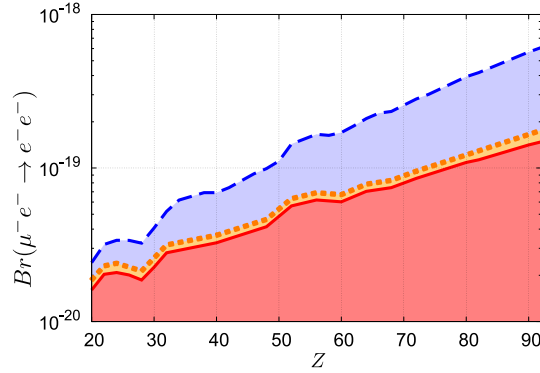


FIG. 4. Upper limits on $Br(\mu^-e^- \rightarrow e^-e^-)$, constrained by the experimental upper limits of $Br(\mu^+ \rightarrow e^+\gamma) < 4.2 \times 10^{-13}$ [1]. The dashed (blue) curve shows the result of previous work [6]. Our results including only the 1S electrons and all the 1S electrons are shown by the solid (red) and the dotted (orange) lines, respectively.

B. Distinguishing mechanisms of CLFV interactions

Having completed to study the $\mu^-e^- \rightarrow e^-e^-$ process for both the contact and the photonic interactions, we study a possibility to distinguish the CLFV mechanism of the $\mu^-e^- \rightarrow e^-e^-$ process in muonic atoms. For this purpose we

consider four simplified models: (i) contact interaction, where the electrons are emitted with the same chirality.

$$g_1 \neq 0, \quad A_{L/R} = 0, \quad \text{and} \quad g_{j \neq 1} = 0, \quad (33)$$

(ii) contact interaction, where the electrons are emitted with opposite chirality.

$$g_5 \neq 0, \quad A_{L/R} = 0, \quad \text{and} \quad g_{j \neq 5} = 0, \quad (34)$$

(iii) photonic interaction

$$A_L \neq 0, \quad A_R = 0, \quad \text{and} \quad g_i = 0. \quad (35)$$

(iv) both of contact and photonic interactions

$$g_1 = 100A_L \neq 0, \quad A_R = 0, \quad \text{and} \quad g_{j \neq 1} = 0. \quad (36)$$

We have chosen $g_1/A_L = 100$ in the model (iv), while $g_1/A_L \sim 270$ using the current upper limits of A_L and g_1 . The Z dependence of $\mu^-e^- \rightarrow e^-e^-$ is shown in Fig. 5. The ratios of the models (i) (in a solid line) and (ii) (in a dashed line) strongly increase as Z . One would need precise measurements to discriminate the model (i) from (ii). On the other hand, the model (iii) exhibits a moderately increase as Z . We may expect the contribution from both the photonic and the contact interactions in the model (iv) and the Z dependence is drawn as a dotted line in Fig. 5. Thus, we can distinguish the CLFV interactions and their dominance by the Z dependence of $\mu^-e^- \rightarrow e^-e^-$.

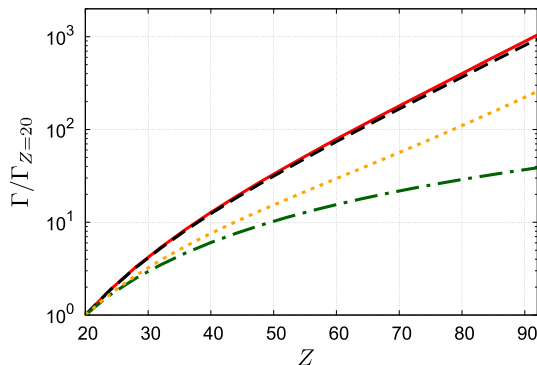


FIG. 5. Z dependence of $\mu^-e^- \rightarrow e^-e^-$ generated by four different models. They are normalized by the rate for $Z = 20$. A solid red line shows the case of model (i), a dashed black line shows that of model (ii), a dash-dotted green one shows that of model (iii), and a dotted orange one shows that of model (iv).

The energy and angular distributions of the emitted electrons also depend on the mechanism of the CLFV interaction. The differential rate of the photonic interaction (model (iii)) and the contact interaction (model (i)) are shown in Fig. 6 and Fig. 7, respectively. The tail distributions of backward electrons for the contact interaction are more frequent than for the photonic interaction. The difference between the model (i) and (ii) appears only when the two electrons are ejected in the same direction ($\cos \theta \sim 1$), where the Pauli principle is most effective, as discussed in [9]. The distribution of the emitted electrons and the Z dependence of the rate would be useful to identify the mechanism of the CLFV interactions contributing to $\mu^-e^- \rightarrow e^-e^-$.

IV. SUMMARY

We have analyzed the $\mu^-e^- \rightarrow e^-e^-$ CLFV process in muonic atoms. Together with our previous analysis [9] for the contact interaction and the present work for the photonic interaction, we find that the relativistic treatment of the emitted electrons and bound leptons is essentially important for their qualitative understanding the rate, in particular the atomic number Z dependence of the rate and the angular and energy distribution of electrons. The Z dependence of the $\mu^-e^- \rightarrow e^-e^-$ rate and the distributions of emitted electrons would be useful to distinguish between the photonic and the four Fermi contact CLFV interactions. So far one cannot distinguish the g_1 term from the g_2 term by using these observables. Therefore the chiral structure of the CLFV interaction should be explored and it would be discussed in our future works.

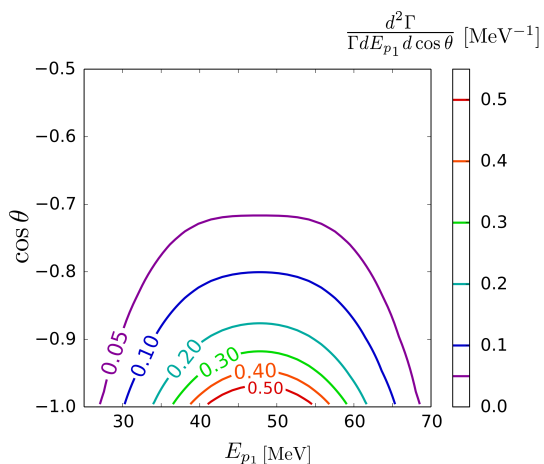


FIG. 6. The double differential rate in model (iii) for ^{208}Pb .

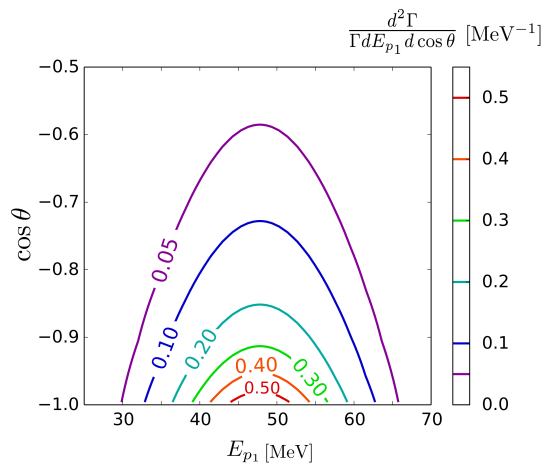


FIG. 7. The double differential rate in model (i) for ^{208}Pb . This figure is printed in Ref. [9].

ACKNOWLEDGMENTS

This work was supported by the JSPS KAKENHI Grant No. 25105009 (J.S.), No. 25105010 and 16K053354 (T.S.), No. 25000004 (Y.K.), No. 16K05325 and 16K17693 (M.Y.). We thank Dr. A. Sato for his fruitful discussions.

Appendix A: Lepton wave functions

The lepton wave functions used in our works are given for its completeness[9]. The scattering state of an electron with its momentum p and its z -component of spin s for the incoming boundary condition can be expressed as

$$\psi_{\mathbf{p},s}^{e(-)}(\mathbf{r}) = \sum_{\kappa,\nu,m} 4\pi i^{l_\kappa} (l_\kappa, m, 1/2, s | j_\kappa, \nu) Y_{l_\kappa, m}^*(\hat{p}) e^{-i\delta_\kappa} \psi_{p,\nu}^\kappa(\mathbf{r}), \quad (\text{A1})$$

where δ_κ is a phase shift for the partial wave κ . The wave function $\psi_{p,\nu}^\kappa(\mathbf{r})$ is represented by the radial wave function $g_p^\kappa(r)$, $f_p^\kappa(r)$ and the angular-spin wave function χ_κ [10, 11] as follows:

$$\psi_{p,\nu}^\kappa(\mathbf{r}) = \begin{pmatrix} g_p^\kappa(r) \chi_\kappa^\nu(\hat{r}) \\ i f_p^\kappa(r) \chi_{-\kappa}^\nu(\hat{r}) \end{pmatrix}. \quad (\text{A2})$$

Furthermore, the wave function of a bound lepton $l = \mu, e$ is given as

$$\psi_{\alpha,s}^l(\mathbf{r}) = \begin{pmatrix} g_{n,l}^\kappa(r) \chi_\kappa^s(\hat{r}) \\ i f_{n,l}^\kappa(r) \chi_{-\kappa}^s(\hat{r}) \end{pmatrix}, \quad (\text{A3})$$

where s is a z -component of spin of the bound state.

-
- [1] A. Baldini *et al.* (MEG Collaboration), *Euro. Phys. J. C* **76**, 434 (2016).
 - [2] U. Bellgardt *et al.*, *Nucl. Phys. B* **299**, 1 (1988).
 - [3] W. Bertl *et al.*, *Euro. Phys. J. C* **47**, 337 (2006).
 - [4] Y. Kuno and Y. Okada, *Rev. Mod. Phys.* **73**, 151 (2001).
 - [5] T. Mori and W. Ootani, *Prog. Part. Nucl. Phys.* **79**, 57 (2014).
 - [6] M. Koike, Y. Kuno, J. Sato, and M. Yamanaka, *Phys. Rev. Lett.* **105**, 121601 (2010).
 - [7] R. Abramishili *et al.*, COMET Phase-I Technical Design Report, KEK Report 2015-1 (2015).
 - [8] A. Abada, V. De Romeri and A. M. Teixeira, *J. High Energy Phys.* 02 (2016) 083.
 - [9] Y. Uesaka, Y. Kuno, J. Sato, T. Sato, and M. Yamanaka, *Phys. Rev. D* **93**, 076006 (2016).
 - [10] M. E. Rose, *Relativistic Electron Theory* (John Wiley & Sons, New York, 1961).

- [11] M. E. Rose, *Elementary Theory of Angular Momentum* (John Wiley & Sons, New York, 1957).
- [12] O. Shanker, Phys. Rev. D **20**, 1608 (1979).
- [13] T. Suzuki, D. F. Measday, and J. P. Roalsvig, Phys. Rev. C **35**, 2212 (1987).